

# Raman Scattering Characterization and Electron Phonon Coupling Strength for MeV implanted InP(111)

D. Paramanik and S. Varma\*

*Institute of Physics, Bhubaneswar - 751005, India.*

## Abstract

Structural modifications in InP(111) due to 1.5 MeV implantation of Sb have been characterized using first order and second order Raman spectroscopy. With both Longitudinal Optical (LO) and Transverse Optical (TO) modes allowed for InP(111), we have investigated the evolution of both these modes as a function of fluence. Intensity, linewidth and shifts of the phonons, for both first order and second order Raman modes, display the increase in damage in the lattice with increasing fluence. The results suggest that the presence of a charge layer in the vicinity of the surface may be effecting the first order Raman data. A LO phonon-plasmon coupled mode, due to the charge layer, has also been observed that becomes sharper and more intense with increasing fluence. Results also show the presence of tensile stress along with the coexistence of crystalline InP regions and amorphous zones in the lattice. Consequently phonon confinement is observed. Phonon Confinement model (PCM) has been applied here to estimate the coherence length and the size of nano-crystalline zones in InP lattice after implantation. A crystalline/ amorphous (c/a) phase transition is observed at the fluence of  $1 \times 10^{14} \text{ ions/cm}^2$ . The electron-phonon coupling strength has been measured by utilizing the second order Raman modes. This coupling strength is seen to decrease as the nano-crystalline zones, in the implanted lattice, become smaller.

PACS numbers: 61.46.+w, 61.72.Vv, 78.30.Fs, 63.22.+m

Keywords: Nanoscale Structures, Ion Implantation, Raman Scattering, Electron-phonon coupling.

---

\*Corresponding author: shikha@iopb.res.in, tel:91-674-2301058, FAX: 91-674-2300142

# 1 Introduction:

Unique properties of InP have attracted enormous interest. It is being widely applied in high speed electronic and optoelectronic devices due to its attractive electronic properties [1, 2, 3] as well as its excellent lattice match with low band gap alloys like GaInAs, GaInAsP, AlGaInAs etc. GaInAsP/InP based photo-diodes operate in low loss window of silica fibers with high quantum efficiency and fast response time. Due to its excellent physical properties like high thermal conductivity, high peak velocities for electrons and holes, InP is considered an important semiconductor material and it is being prominently utilized in the devices for high electron mobility transistors, high efficiency and high speed quantum well lasers, photo-detectors, photonic integrated circuits etc. InP is also preferred, over GaAs based devices, for Millimeter-wave sources and amplifiers due to its low noise and higher efficiency operations in high frequency regime. Junction field effect transistors fabricated on InP display high performance. Sb is considered an important dopant because of its role in the development of field effect transistors and infrared detectors [4]. Sb has also found applications as isoelectronic dopant for trapping charge carriers in InP [5]. Ion-beam implantation techniques are extensively utilized for device processing in semiconductor industry. This is an attractive technique as it provides well controlled and sharp dopant profiles. Due to its low thermal stability, MeV ion implantation is a prominent way to introduce and dope the materials in InP. MeV ion implantation offers a means of doping relatively thicker buried layers with modified properties as well as modifications of vertically limited layers and quantum well structures. The increased density in VLSI circuits also makes the technological applications of the ion implantation, especially in MeV energy range, increasingly important. MeV implantation, however, can also produce damage and can cause severe modifications in the material depending on the nature and the energy of the impinging ion, and the implantation dose [6, 7]. Hence, for ion implantation to be a viable candidate for the development

in semiconductor technology, it is important to understand and characterize the bulk and surface disorder. In earlier studies we have applied Scanning Probe microscopy to investigate the surface modifications on Si(100) [8] and InP(111) [9]. For investigating bulk lattice modifications Raman scattering intensity, half width and peak shift of the zone center phonons are considered very sensitive. Our earlier study of MeV implantation in Si [10] had shown that the Raman scattering is a powerful technique for investigating and monitoring the implantation induced lattice modifications.

During implantation, a projectile while moving forward produces vacancies and interstitials, loses energy primarily due to electronic encounters and is finally deposited at its range governed by its mass and implant energy [11]. At MeV energies, nuclear energy loss ( $S_n$ ) processes are expected to be dominantly responsible for the material modifications. Defects and strains can get produced, via  $S_n$ , causing the modifications in properties of host material [12, 7]. Formation of defects as well as the presence of impurity atoms can lead to stress in the planes of the single crystal or changes in the force constants. Corresponding shifts in the phonon frequencies are reflected in the Raman spectra. Moreover, the damage produced due to defects can cause phonon confinement leading to a reduced phonon coherence length as  $k=0$  selection rule is relaxed, giving rise to an asymmetric broadening in Raman peak. The Raman spectrum thus contains signature of both: the stress and the reduced phonon coherence length due to disorder in the lattice. Raman Scattering, thus, is a powerful tool for investigating and monitoring the radiation induced lattice modifications during ion implantation.

For III-V semiconductors like InP and other zinc-blend structures, the first order Raman spectrum consists of usually two Raman modes corresponding to the Longitudinal Optical (LO) and Transverse Optical (TO) phonons associated with the Brillouin zone center. The zone center phonons corresponding to TO and LO modes obey the following selection rules for zinc blend type crystals. For the scattering by

(111) face, both LO and TO modes are allowed in Raman scattering. However, only TO mode is allowed for scattering by (110) face whereas only LO mode is allowed for (100) face. Both LO and TO modes being allowed for InP(111), we have been able to investigate the evolution of both these modes as a function of ion fluence after MeV implantation. A few studies have investigated the modifications in InP crystals after implantations by Raman scattering technique[13, 14, 15, 16, 17, 18, 19, 20, 21, 22]. However, all these studies investigated the (100) InP where TO mode is forbidden. Moreover, in all these studies keV implantation energies were applied for lattice modifications. There is one report on Raman scattering study of ion modification in InP(111) but for low energy keV implantation with He ions [15].

For InP, phonon dispersion studies indicate [23, 24] that LO branch is almost as flat as TO branch for the entire Brillouin zone. Moreover, Overlap Valence Shell Model [24] results display two very sharp and well separated features corresponding to second order 2LO and 2TO phonon modes with high density of states around  $TO(\Gamma)$  and  $LO(\Gamma)$ . Consequently, second order phonon studies of InP can be effectively undertaken. These second order modes are considered to be more sensitive probes, compared to first order, of lattice disorder, stress and lattice modifications after implantation [14]. However, very few studies have investigated these second order Raman modes [14, 17, 18, 19, 21]. Moreover, all of these studies have investigated InP(100) after keV implantations. There are no studies in literature where second order Raman modes have been investigated after keV or MeV implantation of InP(111) crystals.

At the surface of III-V semiconductor compounds a space charge layer, concentration of high mobility free-electron gas, may exist. If the frequency of this free-electron plasma excitations - plasmons is close to the frequency of LO phonons, the two excitations can interact via their macroscopic electric fields and can form LO phonon-plasmon coupled (LOPC) mode. In n-type InP(100), an intense and well

defined  $L^-$  feature due to LOPC mode has been observed [13]. A few studies have investigated the scattering of light by free carriers in zinc-blende semiconductors [25] and some models have been proposed that analyze the coupling between LO phonons and plasmons. However, there are very few reports for doped InP crystals [13] and none of these studies focus on the evolution of LO-plasmon coupling in InP(111) after implantation. The presence of charge layer also results in a smaller scattering volume near the surface and affects the characteristics of first order LO Raman mode. The second order Raman modes do not suffer from this drawback.

Electron-phonon coupling is a very important factor in understanding the non-linear optical properties of the crystalline materials. For polar materials, the dominant coupling is Fröhlich type between the field induced by the vibrational modes and the electronic charge density [26]. Systematic trends in the electron-phonon coupling strengths, with size, have been seen for Quantum Dots of InP by utilizing second order Raman Scattering [27]. However, there are no studies in literature where electron-phonon coupling strengths have been measured after ion implantation.

In the present study we have utilized first and second order Raman scattering phonon spectra to investigate the lattice modifications in InP(111) after implantation with 1.5 MeV  $Sb^{2+}$  ions. We have studied the evolution of both TO and LO modes as a function of ion fluence. Even at the fluence of  $1 \times 10^{11}$  ions/cm<sup>2</sup>, modifications in first order as well as second order modes demonstrate the initiation of some damage in InP(111) lattice. Once this occurs, a coexistence of nanocrystalline regions and amorphous zones is observed which leads to the confinement of phonons. An estimation of the phonon coherence length has been done by applying the Phonon Confinement Model (PCM) [28] to the first order Raman peak. Existence of a completely amorphous lattice is noticed for a fluence of  $1 \times 10^{14}$  ions/cm<sup>2</sup> and higher.

The evolution of LOPC mode,  $L^{-1}$ , has also been studied as a function of ion fluence. We have also investigated here the effect of implantation on the electron

phonon coupling in InP(111) by utilizing the second order Raman modes. We find that the strength of coupling reduces as the size of nano-crystalline zones, in the implanted lattice, decrease.

Experimental procedures and results are discussed in section 2 and 3, respectively. Conclusions are presented in section 4.

## 2 Experimental

A mirror polished (111)-oriented InP single crystal wafer was used in the present study. The samples were implanted at room temperature with a scanned beam of 1.5 MeV  $\text{Sb}^{2+}$  ions at various fluences ranging from  $1 \times 10^{11}$  to  $5 \times 10^{15}$  *ions/cm*<sup>2</sup>. The average Sb flux was 0.002 to 0.02  $\mu\text{A/cm}^2$ . This current was measured directly on the target after suppressing the secondary electrons by applying a negative bias of 200V to a suppressor assembly around the target. The implantation were performed with the samples oriented  $7^\circ$  off-normal to the incident beam to avoid channeling effects. Monte Carlo simulations were performed for 1.5 MeV Sb implantation in InP using the SRIM'03 code and the mean projected range of Sb-ion distribution was found to be 400 nm [29].

Raman scattering measurements were performed using a SPEX 1877E Triplemate Spectrometer with a liquid nitrogen cooled, charged coupled device array. The laser power was controlled to avoid laser annealing effect on the sample. Raman experiments were carried out at room temperature using the 514 nm line of an argon ion laser in the backscattering geometry. At this wavelength the penetration depth of the light is estimated to be about 100 nm. All the spectra were acquired in the backscattering geometry.

### 3 Results and Discussion

Figure 1 shows the as-implanted first order Raman Spectra from the InP(111) samples implanted at various fluences. The spectrum from a virgin (un-implanted) InP is also shown. The spectra have been shifted vertically for clarity, but the intensity scale is the same for all the spectra. The spectrum of the virgin InP (Fig.1a) shows the characteristic LO and TO Raman modes of crystalline InP(111) [30]. The features at  $305\text{ cm}^{-1}$  and at  $347\text{ cm}^{-1}$  are assigned to the TO and the LO phonon modes, respectively. For the virgin InP(111) we also observe an additional  $L^-$  mode, near  $320\text{ cm}^{-1}$ , as a shoulder near TO mode. This broad phonon feature can be assigned as  $L^-$  LO - phonon plasmon coupled (LOPC) mode. It is well known that in polar semiconductors, like InP, free charge couples with LO modes and forms LOPC-like modes[25]. For InP(100) where TO mode is forbidden,  $L^-$  mode has been observed as sharp feature near  $306\text{ cm}^{-1}$  [20] as well as at  $308\text{ cm}^{-1}$  [31].

The sequence of spectra in Fig. 1 gradually evolve with increasing Sb fluence. The Raman spectrum from a sample implanted with  $1 \times 10^{11}\text{ ions/cm}^2$  shows broader LO and TO modes (Fig. 1b) compared to the virgin sample. Both the features now also exhibit decreased intensity and increased asymmetry. Moreover, both LO and TO modes, after implantation, are shifted towards lower wave numbers compared to the modes in the virgin InP. All these changes reflect the modifications in the InP lattice due to the defects created during implantation. With increasing fluence, we observe a further decrease in intensity of the TO and LO modes. For n-type InP, formation of a charge layer, near surface [14, 30], can result in a smaller scattering volume, thus effecting the intensity of LO mode.

We observe softening as well as asymmetrical broadening in both LO and TO modes with increasing fluence. Both the modes exhibit shifts towards lower wave numbers. The shifts in the peak positions of Raman spectra can be affected by the residual stress as well as by phonon confinement. The contributions due to the two

effects can however be deconvoluted [32]. Spatial Correlation model related to  $k$ -vector relaxation induced damage shows [33] that when disorder is introduced into the crystal lattice by implantation, the correlation function of the phonon-vibrational modes become finite due to the induced defects and consequently the momentum  $k = 0$  selection rule is relaxed. Consequently, the phonon modes shift qualitatively to lower frequencies and broaden asymmetrically as the ion fluence is increased [10]. The reduction in the intensity, shifts towards lower frequencies as well as the asymmetrical broadening of the features with increasing ion fluence, as observed in Fig. 1, are due to the residual defects created in InP lattice via implantation. Accordingly, these two features are also referred to as DALO and DATO, respectively, for disorder activated (LO) and (TO) modes. For the fluences of  $1 \times 10^{14}$  ions/cm<sup>2</sup> and higher, no DALO or DATO modes are observed in Fig. 1 suggesting that at this stage InP lattice undergoes crystalline/amorphous (c/a) phase transition and becomes amorphized. Our results are in contrast to the studies of 150 keV Si<sup>+</sup> [18] or 80 keV Mg [17] implantation in InP(100) where no noticeable changes compared to the virgin were seen upto the fluence of  $1 \times 10^{12}$  ions/cm<sup>2</sup> and the first signatures of disorder were observed after the fluence of  $5 \times 10^{12}$  ions/cm<sup>2</sup>. In contrast to these studies, for keV implantation of Zn in InP(100), c/a transition was seen at a fluence of  $1 \times 10^{13}$  ions/cm<sup>2</sup> [19], which is surprisingly lower than the fluence of c/a transition in the present study. For 2 MeV Se implantation in InP(100), some damage after  $1 \times 10^{12}$  ions/cm<sup>2</sup> has been reported using channeling experiments[34].

The overall Raman scattering, after implantation, is influenced by the presence of the damaged/amorphised zones that get formed in the crystalline lattice. With increasing fluence, the crystalline regions reduce in size whereas the amorphous and damaged zones grow bigger. The disorder is usually a consequence of damage zones that form due to the point defects and/or dislocations created after MeV implantations. At high fluences the damaged zones in the lattice begin to overlap and finally



at sufficiently high fluences  $c/a$  phase transition may occur leading to a completely amorphised lattice [35].

Figure 2 displays the quantitative variations, as a function of ion fluence, in intensity, linewidth and position of first order Raman modes of InP(111) after Sb implantation. In Fig. 2a the Raman intensity for TO and LO modes, normalized with respect to the intensity from the virgin sample, are shown. For both the modes, we observe a decrease in intensity for increasing fluence. For TO mode, however, the decrease is larger and faster. The widths (FWHM) for both the modes are shown in Figure 2b. We observe an increase in the linewidths for both the modes as the fluence is increased. Again, the increase is more pronounced in TO mode. The widths of TO and LO modes, after the fluence of  $1 \times 10^{13} \text{ ions/cm}^2$ , are  $30$  and  $20 \text{ cm}^{-1}$ , respectively. In contrast, much smaller and same linewidths for LO and TO modes ( $\sim 7 \text{ cm}^{-1}$ ) have been observed after keV implantation at this fluence [15].

The positions of the LO and TO modes are shown in Figs. 2c and 2d, respectively. Although for the virgin sample the positions for LO and TO modes were  $347$  and  $305 \text{ cm}^{-1}$ , respectively, after the fluence of  $1 \times 10^{13} \text{ ions/cm}^2$  these mode appear at  $339$  and  $298 \text{ cm}^{-1}$ , respectively. The overall shift ( $\omega$ ) is larger and increases more rapidly for LO mode. These shifts indicate that the lattice is under stress due to the creation of defects after implantation. Moreover, the shift of LO and TO modes towards the lower wave numbers suggest that the stress is of tensile nature. Surprisingly, although TO mode showed larger variation in intensity and width compared to the LO mode (in fig. 2a,b), the overall shift is larger for LO mode ( $\sim 8 \text{ cm}^{-1}$ ). With LO being a more surface sensitive mode, due to the Fröhlich interactions [36], lower intensity and FWHM of LO mode suggest that the lattice has undergone less modifications on the surface than in bulk. This, however, will lead to a larger stress on the surface. Higher shifts in LO mode show that this is indeed happening. Moreover, the shift being towards the lower wavenumbers suggests that the surface is under large tensile

stress. Similar large shifts, in LO mode, towards lower wave numbers have also been observed for InP Quantum Dots [27].

Figure 3 shows the variations in intensity, width and position of  $L^-$  plasmon-phonon coupled (LOPC) mode as a function of ion fluence. The intensity of  $L^-$  mode increases upto the fluence of  $1 \times 10^{13} \text{ ions/cm}^2$ . For higher fluences,  $L^-$  feature is not visible. As seen in Fig. 1, the c/a transition occurs in InP(111) lattice at the fluence  $1 \times 10^{14} \text{ ions/cm}^2$ . The disappearance of  $L^-$  mode may reflect the capture of free carriers by defects due to the creation of amorphised zones after ion implantation. In Fig 3b, the FWHM of  $L^-$  mode is seen to decrease with increasing fluence. This mode, thus, becomes sharper and more intense with increasing fluence. This is as expected since LOPC can become stronger with increasing carrier density. The position of  $L^-$  mode shifts towards lower wave numbers with the increasing fluence. As expected, the frequency of  $L^-$  mode asymptotically approaches TO frequency [25]. With  $L^-$  occurring at  $320 \text{ cm}^{-1}$  for the virgin sample and at  $316 \text{ cm}^{-1}$  after the fluence of  $1 \times 10^{13} \text{ ions/cm}^2$ , the overall shift is about  $4 \text{ cm}^{-1}$  for this mode.

Figure 4 shows the second order Raman spectra of InP(111) after implantation with Sb ions at various fluences. For the virgin InP(111) a distinct triplet at 617, 650 and 682  $\text{cm}^{-1}$  is observed (fig. 4a). These features correspond to the 2TO, LO+TO and 2LO modes, respectively. The evolution of all these features, as a function of ion fluence, are displayed in fig. 4. It has been shown that the scattering volume for the second-order modes comprises the volume effectively probed by the exciting laser and hence these modes better reflect the nature of lattice modification than first order modes in zinc-blende (100) structures [14]. Figure 5 shows the variations in the intensity, width and position of second order TO and LO modes, as a function of ion fluence. Figure 5a shows the intensity of 2TO and 2LO modes, at various fluences, normalized with respect to the respective intensities from the virgin sample. For both the modes, we observe a reasonable decrease in intensity at the

fluence of  $1 \times 10^{11}$  *ions/cm<sup>2</sup>*. This result is in contrast to previous studies after keV implantation in InP(100) where no significant modifications in second order Raman modes were observed below the fluence of  $5 \times 10^{12}$  *ions/cm<sup>2</sup>* [17, 18]. For both 2LO and 2TO modes, we observe a decrease in the intensity with increasing fluence. The reduction of intensity in Fig. 5a, like first order, is again larger for the 2TO mode than for 2LO. Although the overall decrease in intensity for LO and 2LO modes is similar, 2TO modes exhibit much less decrease compared to TO mode. At  $1 \times 10^{13}$  *ions/cm<sup>2</sup>*, we observe that for TO and 2TO modes the intensities are respectively about 25% and 50% of the intensity from virgin sample. Figure 5b shows the widths (FWHM) of 2TO and 2LO features. The widths of 2LO and 2TO modes, for the virgin InP(111), are observed to be 10 and 15  $\text{cm}^{-1}$ , respectively. These widths are slightly smaller than those observed for virgin InP(100) where widths for LO and TO mode were found to be 12 and 16  $\text{cm}^{-1}$ , respectively [37]. Although 2LO mode is slightly narrower than LO mode for the virgin sample as well as after implantation, the width of 2TO mode is larger than TO mode for the virgin sample. After implantation, the widths of TO and 2TO modes appear similar. Again like first order TO mode, 2TO mode shows larger and more rapid increase in width compared to 2LO mode. The behavior of the shifts in position ( $\omega$ ) of the second order modes is, however, different and unlike first order where LO mode exhibited larger shifts compared to TO mode, 2LO mode shows very little change in its position. Figure 5c shows that 2LO mode experiences only a very slight shift ( $\sim 2$   $\text{cm}^{-1}$ ) towards the lower wave numbers after the fluence of  $1 \times 10^{13}$  *ions/cm<sup>2</sup>* whereas 2TO mode exhibits a large shift of about 7  $\text{cm}^{-1}$  (Fig. 5d). The shifts seen for 2TO mode are similar to those seen for TO mode in Fig. 2d. The modifications in the second-order Raman modes after implantation, like first-order, are associated with the degradation of the crystalline order in the InP(111) lattice.

The second order optic phonon spectra also contains a combination mode of

LO+TO. Figure 6 shows the evolution of this combination mode as a function of ion fluence. The overall intensity of the mode initially increases upto the fluence of  $1 \times 10^{12} \text{ ions/cm}^2$  but decreases for higher fluences. For  $1 \times 10^{14} \text{ ions/cm}^2$ , where c/a transition occurs, and higher fluences the combination LO+TO mode, is no more visible. The FWHM of the combination mode is  $15 \text{ cm}^{-1}$  for the virgin InP(111). This width is larger than the linewidth of combination mode ( $9 \text{ cm}^{-1}$ ) observed for virgin InP(100) [37]. Surprisingly, though combination mode, seen here, is wider than the previous study [37], the 2LO and 2TO modes are narrower in the present study. The linewidth of the combination mode increases with fluence becoming  $30 \text{ cm}^{-1}$  after the fluence of  $1 \times 10^{13} \text{ ions/cm}^2$  (Fig. 6b). The position ( $\omega$ ) of this mode, however, does not show much shift with increasing ion fluence.

During implantation, the lattice ions are displaced, creating defects and disordered regions in the process. With increasing lattice disorder, the phonon coherence length is reduced and  $\mathbf{k}=0$  selection rule is relaxed, giving rise to measurable shifts and asymmetric broadening of the Raman peaks [33]. Due to translational symmetry breakdown, PCM developed by Richter et al. [28] can be used to evaluate the phonon confinement length or the average size of the undamaged crystalline regions. Assuming a constant correlation length  $L$  in the scattering volume, the intensity of the first order Raman band in the scattering volume is given by

$$I(\omega) = \int_0^{2\pi/a_0} \frac{|C(q)|^2 4\pi q^2 dq}{[\omega - \omega(q)]^2 + (\Gamma_0/2)^2} \quad (1)$$

where  $a_0$  is the lattice constant of InP ( $5.586 \text{ \AA}$ ).  $\Gamma_0$  is the Raman intrinsic line width of the crystalline InP having values of  $10.5$  and  $7.6 \text{ cm}^{-1}$  for TO and LO modes, respectively. The weight factor  $C(q)$  for the scattering with wave vector  $q$  is given by

$$|C(q)|^2 = \exp\left(\frac{-q^2 L^2}{16\pi^2}\right) \quad (2)$$

and the phonon dispersion relation is given by [38]

$$\omega(q) = \omega_A - \omega_B(q/q_0)^2 \quad (3)$$

where  $\omega_A$  is the wave vector of the first order Raman band in the absence of disorder effects and  $q_0 = \frac{2\pi}{a_0}$ . Neutron scattering data provides  $\omega_B$  to be 42 and 68  $\text{cm}^{-1}$ , respectively, for LO and TO modes [23].

By fitting the experimental LO and TO Raman modes with PCM we have obtained the phonon coherence length, L, of the as implanted samples. Figure 7 shows the results of fittings of PCM model to LO mode of Raman spectra, along with respective L values, at various fluences. Raman LO mode from the virgin InP sample is symmetric with an infinite coherence length. A fluence of  $1 \times 10^{11} \text{ ions/cm}^2$ , causes an asymmetry in the LO mode which can be due to the presence of some disordered or amorphous regions in the InP sample that are large enough for phonon confinement. By utilizing PCM, a phonon coherence length of 66 Å is obtained, indicating the presence of undamaged InP zones with average crystallite size of this dimension. The shape of Raman LO mode after the fluence of  $1 \times 10^{12} \text{ ions/cm}^2$  shows a very slight increase in asymmetry compared to that observed at  $1 \times 10^{11} \text{ ions/cm}^2$  and displays a coherence length of 56 Å. A highly asymmetric Raman LO mode is observed after the fluence of  $1 \times 10^{13} \text{ ions/cm}^2$ . The phonon coherence length at this stage is only 35 Å. Thus, results after PCM fitting, for the fluences  $1 \times 10^{11} \text{ ions/cm}^2$  to  $1 \times 10^{13} \text{ ions/cm}^2$ , suggest the presence of nanometer sized undamaged crystalline regions in the as-implanted InP matrix. Thus, a coexistence of nanocrystalline structures as well as amorphous InP matrix takes place at these fluences. For higher fluences the InP lattice becomes completely amorphous. It is likely that the small amorphous zones inflate in size or some new amorphous zones get created with increasing fluence that finally overlap leading to total amorphization of the lattice.

In Fig. 7 we observe a coherence length of 35 Å at  $1 \times 10^{13} \text{ ions/cm}^2$ . At this fluence, first order LO mode displays an overall shift of 8  $\text{cm}^{-1}$  and a width of 21  $\text{cm}^{-1}$

(see Fig. 2). Surprisingly, keV implantation at  $1 \times 10^{13} \text{ ions/cm}^2$  in InP(100), also leads to a similar coherence length ( $\sim 36 \text{ \AA}$ )[20]. However, shift, in LO mode, was only  $1.3 \text{ cm}^{-1}$  whereas FWHM was  $18 \text{ cm}^{-1}$ . For InP quantum dot (QD) of  $35 \text{ \AA}$  the shifts and FWHM of LO mode are found to be  $\sim 4 \text{ cm}^{-1}$  and  $\sim 20 \text{ cm}^{-1}$ , respectively [27]. Although the width of LO mode in the present study as well as in studies by Yu et al. [20] and Seong et al.[27] are similar, the shifts for same coherence length of  $35 \text{ \AA}$ , are very different. Varying LO shifts may indicate varying order of associated stresses. After MeV implantation of Sb in Si [10] the coherence length was found to be  $330 \text{ \AA}$  for a fluence of  $1 \times 10^{13} \text{ ions/cm}^2$ . Higher nuclear energy loss,  $S_n$ , for Sb in InP (1.9 keV/nm) compared to that in Si (1.2 keV/nm) will be responsible for the smaller nano-crystalline zones in InP at all fluences.

The electron-phonon coupling strength can be estimated by measuring the normalized Raman intensity ( $I_R$ ) of the 2LO phonon with respect to that of LO phonon.  $I_R$  is considered approximately proportional to the electron-LO phonon coupling [26, 39]. We have obtained  $I_R$  for virgin InP(111) as well as after implantation at various fluences and have shown them in Fig. 8. Furthermore, in Fig. 8 (top axis) we have also marked the coherence length,  $L$ , as obtained from the fitting results of PCM model (shown in Fig. 7) at all fluences. For virgin InP(111) we find  $I_R$  of 0.20 in Fig. 8. The  $I_R$  is seen to decrease as the fluence is increased. We observe  $I_R$  of 0.17, 0.16 and 0.13 for the fluences of  $1 \times 10^{11}$ ,  $1 \times 10^{12}$  and  $1 \times 10^{13} \text{ ions/cm}^2$ , respectively. From the PCM fitting results we had found that the coherence length of the crystalline zones is  $66 \text{ \AA}$  at the fluence of  $1 \times 10^{11} \text{ ions/cm}^2$  (Fig. 7). It was also observed that as the fluence is increased, the coherence lengths decrease and become  $56 \text{ \AA}$  and  $35 \text{ \AA}$  for the fluences of  $1 \times 10^{12}$  and  $1 \times 10^{13}$ , respectively. Thus, from Fig. 8 it is observed that the electron- phonon coupling strength of nano-crystalline zones in InP decreases as their sizes decrease. This behaviour is similar to the results seen for InP Quantum dots [27]. However, the  $I_R$  seen for InP QD (0.13 for  $55 \text{ \AA}$  and 0.08 for  $35 \text{ \AA}$ ) were very

slightly smaller than those seen here for nano-crystalline zones created after MeV implantation. In the present study we observe that the electron-phonon coupling,  $I_R$ , is largest for the virgin bulk-InP which also has biggest coherence length. With the decrease in coherence length, the electron-phonon coupling strength also decreases. The strength of coupling is about 1.5 times weaker in the nano-crystalline zones, of  $35\text{\AA}$  size, than in the bulk -InP. This reduction in coupling is consistent with the increased overlap of electron and hole when there is substantial quantum confinement as also observed for bulk CdSe Quantum dots [26] where a 20 times reduction in coupling strength, compared to bulk solid, was observed for a  $45\text{\AA}$  cluster. However, for InP quantum dots [27], inexplicable reverse result with smallest  $I_R$  of 0.06 for the bulk-InP was seen.

## 4 Summary and Conclusion

InP(111) lattice, after MeV implantation, has been investigated by first and second order Raman Spectroscopy. Evolution of both TO and LO modes as a function of ion fluence has been studied. The first order results are influenced by the presence of a charge layer in the vicinity of surface. LO-phonon plasmon coupled mode,  $L^-$ , is seen to become stronger with increasing ion fluence. Results indicate coexistence of nanocrystalline zones and amorphous regions in the implanted InP lattice. Electron-Phonon coupling strength in nano-crystalline zones has been estimated and it reduces as the size of the crystalline regions decreases with increasing fluence. PCM has been applied to estimate the coherence length due to the confinement of phonons in the implanted lattice and nano-crystalline zones of dimensions smaller than  $66\text{\AA}$  have been observed.

## 5 Acknowledgments

This work is partly supported by ONR grant no. N00014-97-1-0991. We would like to acknowledge the help of A. Pradhan in Raman scattering measurements. We would also like to thank Prof. S.N. Behera for useful discussions.



## References

- [1] D. Streit, Compound Semiconductors, May 2002.
- [2] B. Humphreys, A. O'Donnell, Compound Semiconductors, August 2003.
- [3] D. Lammers, Electronic Engineering Times, 12 September 2002.
- [4] G. Tempel, N. Schwarz, F. Muller, F. Koch, H.P. Zeindl, and I. Eisele, Thin Solid Films **174** (1990) 171.
- [5] S.G. Bishop, B.V. Shanabrook, P.B. Klein, and R.L. Henry, Phys. Rev. B. **38**, 8469 (1988).
- [6] M. Tamura and T. Suzuki, Nucl. Instr. and Meth. **B39** (1989) 318.
- [7] S. Dey, G. Kuri, B. Rout and S. Varma, Nucl. Instr. Meth. B **142** (1998) 35.
- [8] S. Dey, D. Paramanik, V. Ganeshan and S. Varma, Appl. Surf. Sci. in press (2006)
- [9] D. Paramanik, A. Pradhan, S. Varma, J. Appl. Phys **99**, 014304 (2006).
- [10] S. Dey, C. Roy, A. Pradhan and S. Varma, J. Appl. Phys. **87** (2000) 1110.
- [11] W. K. Chu, J. W. Mayer and M. A. Nicolet, Backscattering Spectrometry (Academic Press, New York, 1978).
- [12] G.K. Mehta, Vacuum **48** (1997) 957.
- [13] L. Artus, R. Cusco, J. Ibanez, N. Blanco, and G.G. Diaz, Phys. Rev. B **60**, 5456 (1999).
- [14] L. Artus, R. Cusco, J. Ibanez, J. M. Martin, G. Gonzalez-Diaz, J. Appl. Phys. **82**, 3736 (1997).

- [15] I.M. Tiginyanu, A.I. Terletsy, V.V. Ursaki, Solid State Commun. **96**, 789 (1995).
- [16] K. Santhakumar, P. Jayavel, R. Kesavamoorthy, P.Magudapathy, K.G.M. Nair, V. Ravichandran, Nucl.Inst. and Meth. B,**194**, 451 (2002).
- [17] J. Ibanez, R.Cusco, N. Blanco, G. Gonzalez-Diaz, L. Artus, Nucl.Inst. and Meth. B,**148**, 454 (1999).
- [18] R. Cusco, G. Talamas, L. Artus, J. M. Martin, G. Gonzalez-Diaz, J. Appl. Phys.**79**, 3927 (1996).
- [19] E. Bedel, G. Landa, R. Carles, J.B. Renucci, J.M. Roquais and P.M. Favennec, J. Appl. Phys. **60**, 1980 (1986).
- [20] Soon Jae Yu, Hajime Asahi, Shuichi Emura, Hitoshi Sumida, Shun-ichi Gonda, and Hisao Tanoue, J. Appl. Phys.**66**, 856 (1989).
- [21] R. Cusco, J. Ibanez, N. Blanco, and G.G. Diaz, L. Artus, Nucl.Inst. and Meth. B,**132**, 627 (1997).
- [22] C.S. Rama Rao, S. Sundaram, R.L. Schmidt, J. Comas, J. Appl. Phys.**54**, 1808 (1983).
- [23] P.H. Borchers, G.F. Alfrey, D.H. Saundersons, and A.D.B. Woods, J. Phys. C: Solid State Phys. **8**, 2022 (1975).
- [24] P.H. Borchers, K. Kune, J. Phys.C: Solid State Phys.**11**, 4145 (1978).
- [25] G. Abstreiter, M. Cardona, A. Pinczuk, in *Light Scattering in Solids IV* edited by M. Cardona and G. Guntherodt, Topics in Applied Physics, Vol. 54 (Springer, Verlag Berlin, 1984) and references therein.
- [26] A.P. Alivisatos, T.D. Harris, P.J. Carroll, M.L. Steigerwald and L.E. Brus, J. Chem Phys. **90** 3463 (1989).

- [27] M.J. Seong, O.I. Micic, A.J. Nozik and A. Mascarenhas, and H.M. Cheong, Appl. Phys. Lett. **82**, 185 (2003).
- [28] H.Richter, Z.P.Wang and L.Ley, Solid State Commun. **39**, 625 (1981).
- [29] J. P. Biersack and L. G. Haggmark, Nucl. Instr. and Meth. **B174**, 257 (1980).  
We have used the version SRIM 03.
- [30] A. Pinczuk, A.A. Ballman, R.E. Nahory, M.A. Pollack, and J.M. Worlock, J. Vac. Sci. Technol., **16** 1168 (1979).
- [31] S.K. Mohanta, R.K. Soni. S. Tripathy and S.J. Chua, Appl. Phys. Lett. **88** 043101 (2006).
- [32] X.Huang, F.Ninio, L.J.Brown and S.Prawer, J. Appl. Phys. **77**, 5910 (1995).
- [33] K.K. Tiong, P.M. Amirtharaj, F.H. Pollak and D.E. Aspnes, Appl. Phys. Lett. **44**, 122 (1984).
- [34] W. Wesch, E. Wendler, T. Bachmann, and O. Herre, Nucl. Instru. Meth. Res. B. **96**, 290 (1995).
- [35] H.Wemple, J.C. North, and J.M. Dishman, J. Appl. Phys.**45**, 1578 (1974).
- [36] K.J. Nash and M.S. Skolnick, Phys. Rev. Lett.**60**, 863 (1988).
- [37] L. Artus, R. Cusco,J.M. Martin, G. Gonzalez-Diaz, Phys. Rev. B.**50**, 11552 (1994).
- [38] Z. Sui, P.P. Leong, I.P. Herman, G.S. Higashi, and H. Temkin, Appl. Phys. Lett.**60**, 2086 (1992).
- [39] J.J. Shiang, R.H. Risbud and A.P. Alivisatos, J. Chem Phys. **98** 8432 (1993).

## Figures:

Fig. 1: First order optical Raman spectra of virgin InP (a) and 1.5 MeV Sb implanted InP at ion fluences of  $1 \times 10^{11}$  *ions/cm<sup>2</sup>* (b),  $1 \times 10^{12}$  *ions/cm<sup>2</sup>* (c),  $1 \times 10^{13}$  *ions/cm<sup>2</sup>* (d),  $1 \times 10^{14}$  *ions/cm<sup>2</sup>* (e),  $5 \times 10^{14}$  *ions/cm<sup>2</sup>* (f) and  $1 \times 10^{15}$  *ions/cm<sup>2</sup>* (g).

Fig. 2: Evolution of first order LO and TO modes: The intensity of both LO and TO modes normalized with respect to virgin (a), FWHM of both LO and TO modes (b) the shift in position of LO mode (c) and shift in position of TO mode (d) are shown as a function of ion fluence. Data for the virgin sample are also shown.

Fig. 3: Evolution of L<sup>-</sup> mode: The intensity normalized with respect to virgin (a), FWHM (b) and the shift in position (c) are shown as a function of ion fluence. Data for the virgin sample are also shown.

Fig.4: Second order optical Raman spectra of virgin InP (a) and 1.5 MeV Sb implanted InP at ion fluences of  $1 \times 10^{11}$  *ions/cm<sup>2</sup>* (b),  $1 \times 10^{12}$  *ions/cm<sup>2</sup>* (c),  $1 \times 10^{13}$  *ions/cm<sup>2</sup>* (d),  $1 \times 10^{14}$  *ions/cm<sup>2</sup>* (e),  $5 \times 10^{14}$  *ions/cm<sup>2</sup>* (f) and  $1 \times 10^{15}$  *ions/cm<sup>2</sup>* (g)

Fig. 5: Evolution of second order 2LO and 2TO modes: The intensity of both 2LO and 2TO modes normalized with respect to virgin (a), FWHM of both 2LO and 2TO modes (b) the shift in position of 2LO mode (c) and shift in position of 2TO mode (d) are shown as a function of ion fluence. Data for the virgin sample are also shown.

Fig. 6: Evolution of LO+TO mode: The intensity normalized with respect to virgin (a), FWHM (b) and the shift in position (c) are shown as a function of ion fluence. Data for the virgin sample are also shown.

Fig.7: Raman spectra of Sb implanted InP(111) at various fluences fitted with PCM as described by Eq.(1). ●: experimental data, -: phonon confinement model fit to data.  $L(\text{Å})$  is the phonon coherence length as determined by the fit to the data. Fitting for the virgin sample is also shown.

Fig.8: Normalized Raman intensity of second-order 2LO phonon with respect to that of first-order LO as a function of ion fluence. Value for the virgin bulk-InP is also shown. The coherence lengths ( $L$ ), at all fluences, are also marked on the top axis.

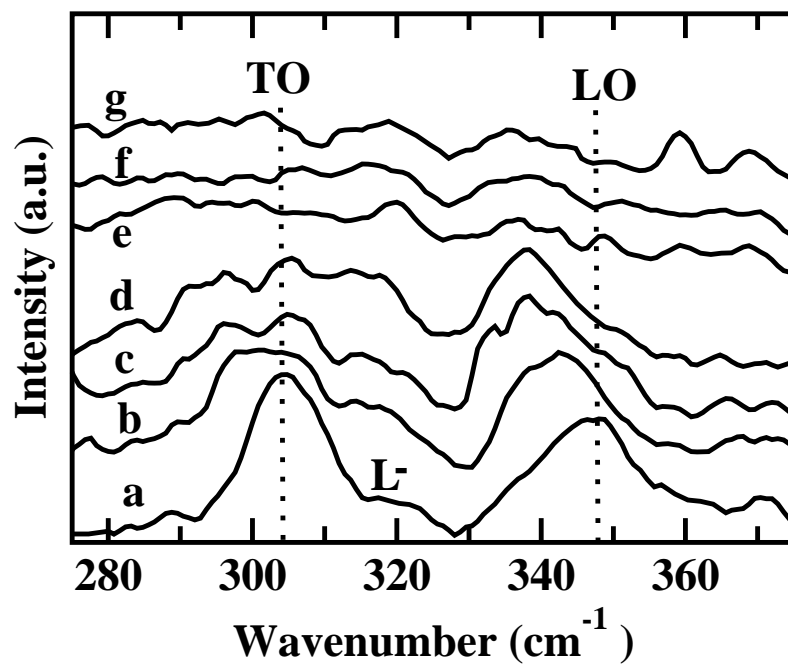


Figure 1:

Paramanik et al.

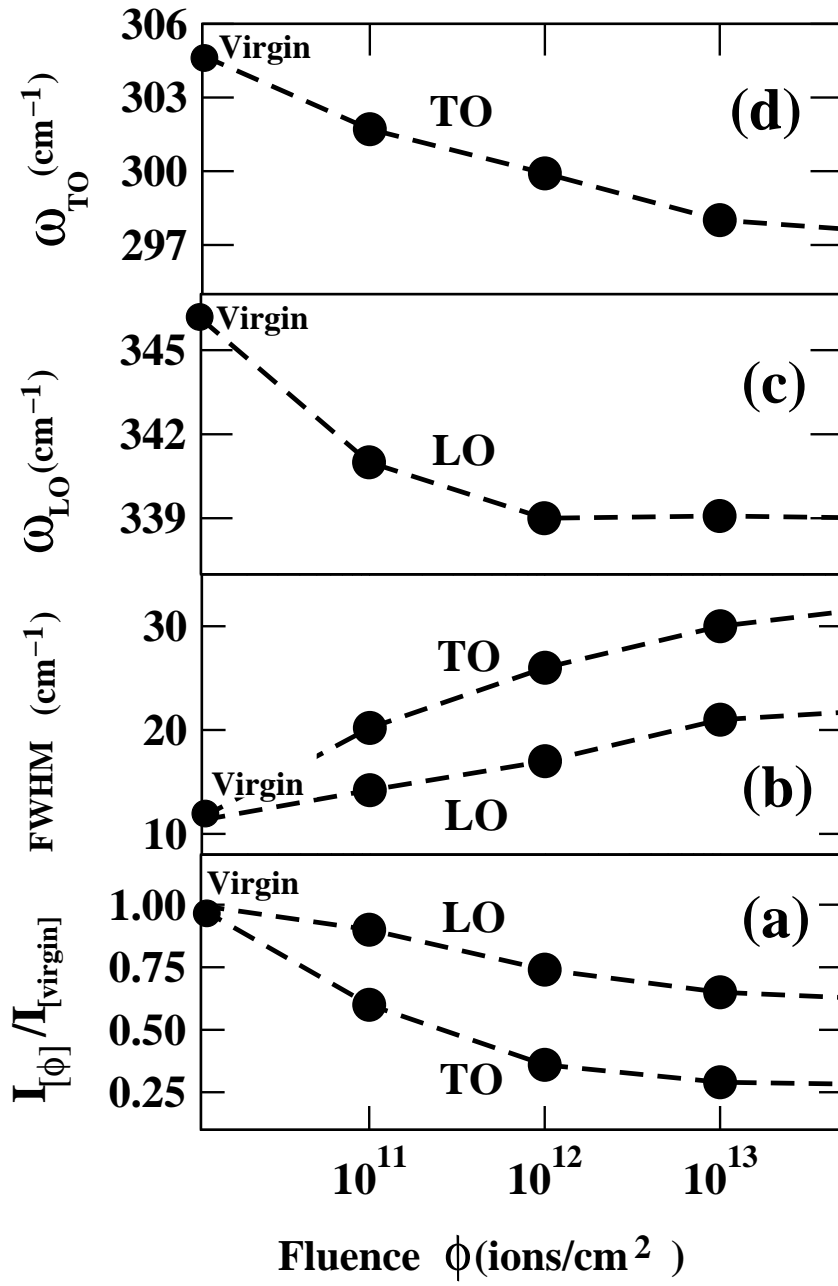


Figure 2:

Paramanik et al.

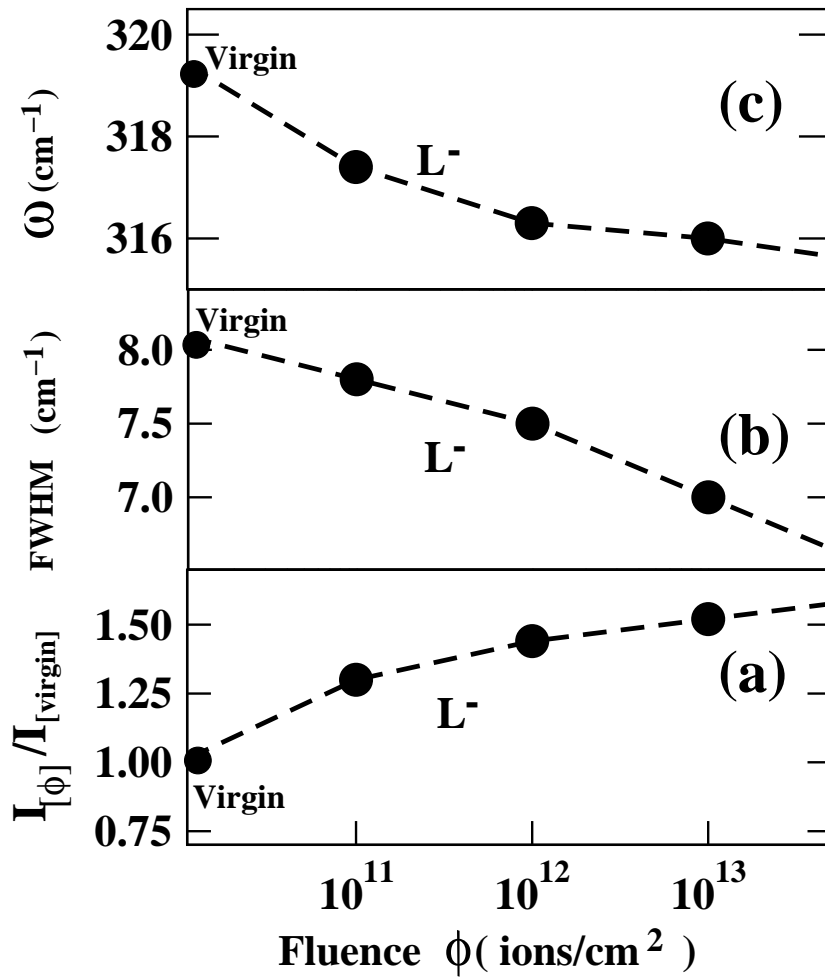


Figure 3:

Paramanik et al.



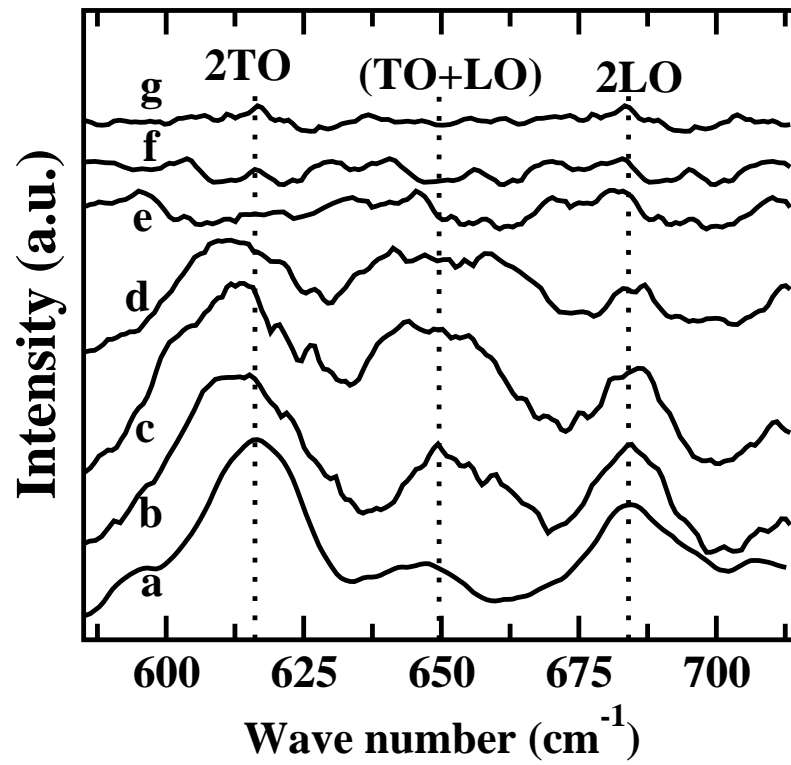


Figure 4:

Paramanik et al.

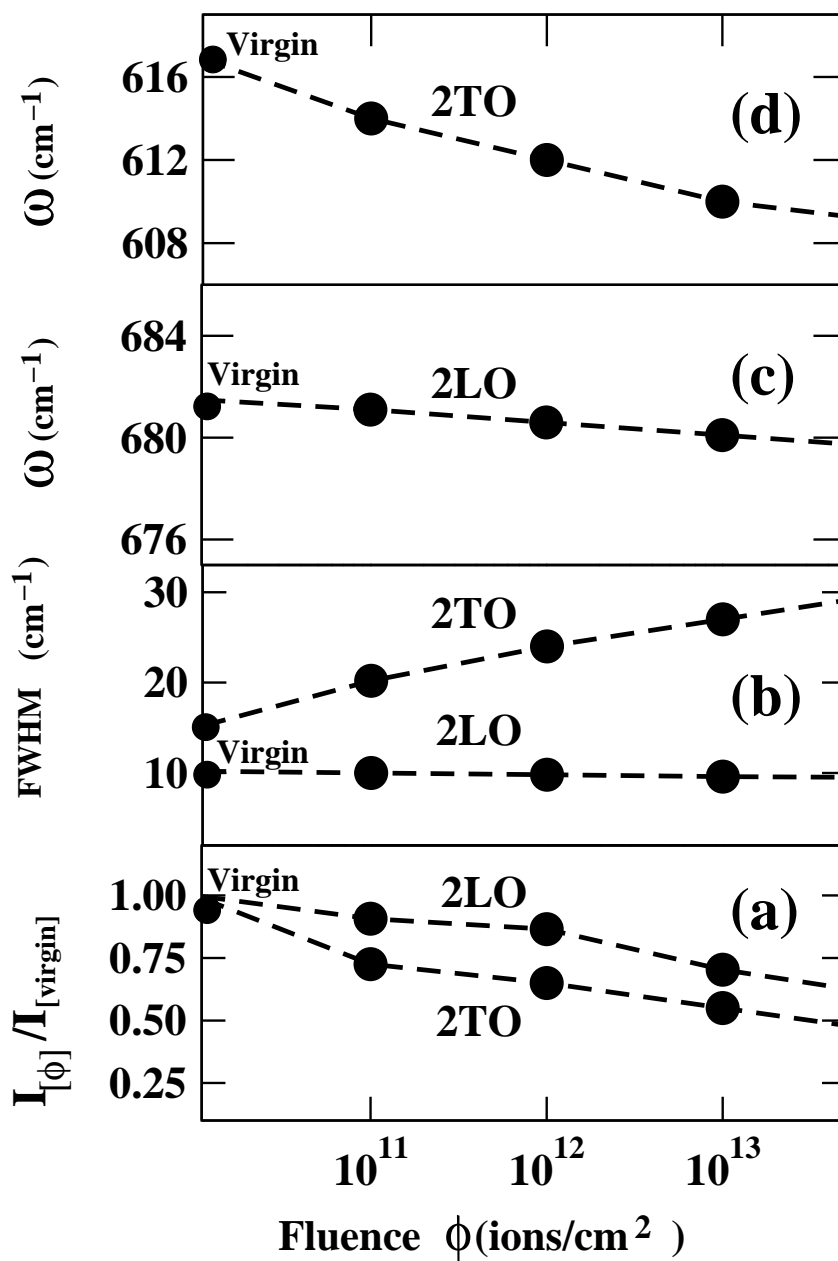


Figure 5:

Paramanik et al.

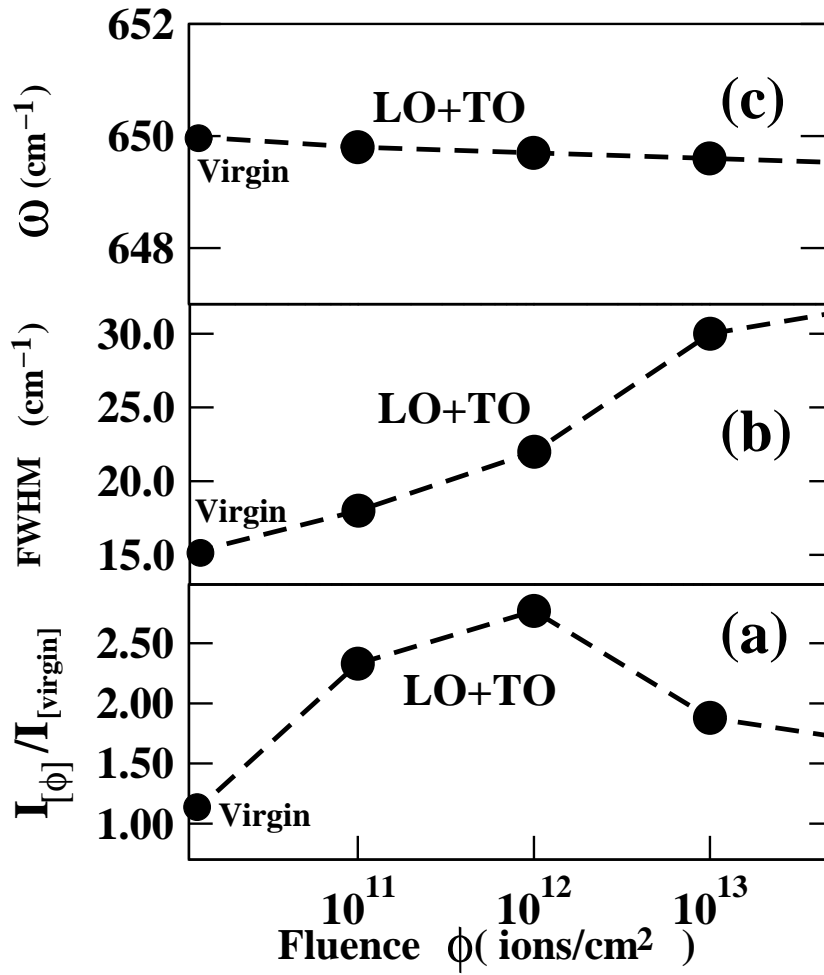


Figure 6:

Paramanik et al.

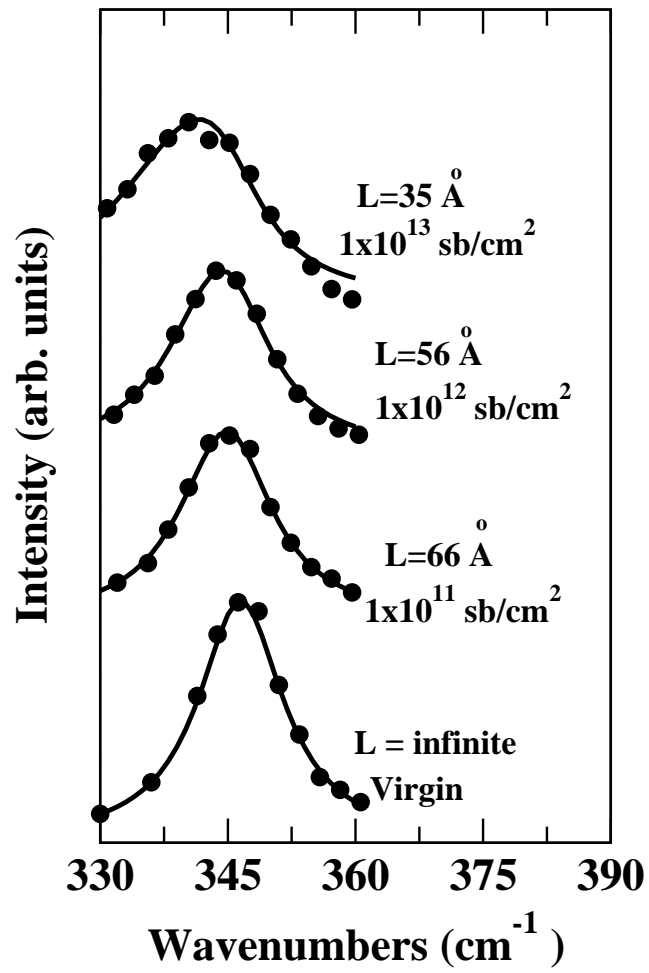


Figure 7:

Paramanik et al.

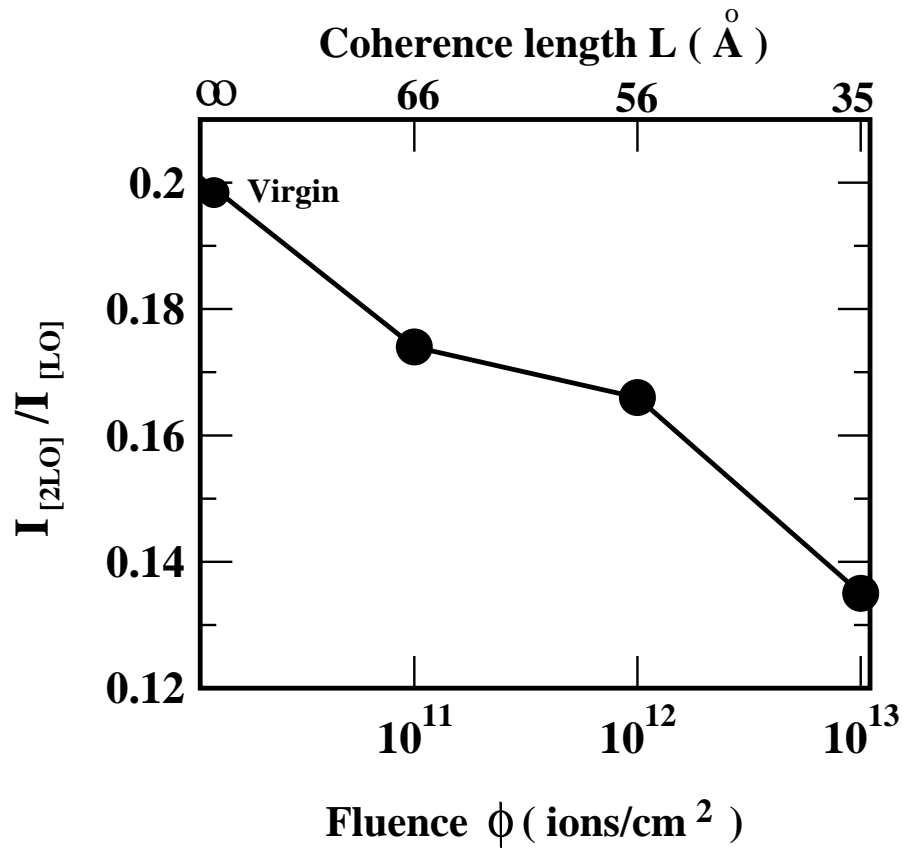


Figure 8:

Paramanik et al.